On-Orbit High-Accuracy Geometric Calibration for Remote Sensing Camera Based on Star Sources Observation

Xuedi Chen, *Graduate Student Member, IEEE*, Fei Xing, Zheng You, Xing Zhong, and Kaihua Qi

***Abstract*— The on-orbit calibration technology for internal and external parameters of remote sensing camera is the key to guaranteeing the imaging quality and positioning accuracy. Conventional landmark-based methods are not suitable for satellite missions where landmarks do not work nor for the on-orbit autonomous calibration of large remote sensing constellation. Hence, we introduced an on-orbit geometric calibration method based on star sources observation. By adjusting the satellite attitude, the camera and star sensor can simultaneously detect the star sources. Taking the star sources as control points, a high-accuracy "camera-star sensor" joint geometric calibration model integrating the space–time effects and optical imaging is established, which precisely decouples the deviations caused by the relativistic effects, the distortion of internal parameters, and the bias of external parameters. Furthermore, the procedures of the method are designed for on-orbit autonomous calibration. On-orbit experiments were carried out in several satellites, such as Jilin-1 ShiPin07 (JL-1 SP07). The results showed that the accuracy of internal calibration could reach 0.052" and the error of external installation matrix was within ±1.4". Therefore, the method is attractive for actualizing on-orbit autonomous geometric calibration accurately and complements the conventional methods where the availability of landmarks is hard.**

***Index Terms*— Astronomical observation, geometric calibration, remote sensing, stellar aberration.**

I. Introduction

REMOTE sensing plays a significant role in multiple fields, such as environmental monitoring, national security, and scientific exploration [1], [2]. High-precision image positioning is an important aspect of remote sensing and has critical requirements for the accuracy of internal parameters and external installation matrix of camera [3], [4]. Generally, the camera is calibrated meticulously in the laboratory before satellite launching. However, the vibration and the changes of environmental conditions during the satellite launching and on-orbit operation will cause considerable drift in the internal and external parameters. Therefore, it is necessary to conduct the geometric calibration on orbit.

Most of the traditional on-orbit calibration methods are based on the images of ground calibration sites captured by camera on orbit [5], [6]. Ground control points (GCPs) obtained by image matching are used to realize the calibration. The IKONOS satellite was equipped with a camera with 1-m resolution and a field angle map (FAM) model was set up to describe the interior orientation of camera. The FAM calibration was implemented over the Denver test range, realizing the residual error below 1 pixel. Then, the interlock angles related to camera and satellite were determined by special MTF GCP [7], [8]. SPOT-5 satellite launched by France used abundant reference data from "supersite." The accuracy of internal parameters was up to 0.12" by the polynomial fitting method. Then, the external installation matrix of camera was calibrated by fusing the attitude data [9], [10]. For the ZiYuan-3 satellite, the internal calibration was carried out over the Anping calibration site, and the accuracy was superior to 0.2 pixels [11]. The methods established upon ground calibration sites are accurate but limited by high maintenance cost, cloud cover, and long temporal interval.

To free from the limitation caused by ground calibration sites, the calibration method based on "cross images" was conducted in the PLEIADES satellite for the first time, which benefited from the improvement of satellite maneuverability [12], [13]. In this method, satellite was adjusted to capture an image pair with an included angle of nearly 90° in the yaw direction. The geometric intersection relationship of light ray in the overlapping part of the image pair was used as a constraint for calibration. Similarly, Pi *et al.* [14] used a series of push-broom images with overlapping portion to calibrate the camera, which was captured in multiple attitudes. This method could obtain more stable images than the swing scanning imaging model of the PLEIADES satellite. These methods are independent of the ground calibration sites and can be executed anywhere on the world in theory.

These landmark-based methods can provide reliable and accurate geometric calibration for most remote sensing satellites [13]–[15]. However, the landmark-based methods are weak in satellite missions where the access of landmarks becomes difficult or even impossible, such as meteorological satellites [16], deep space missions [17]–[20], and night-light satellites [21]. Furthermore, the methods are also inapplicable to on-orbit autonomous calibration because of the difficulty in extracting and matching feature points from ground images. The autonomous calibration is highly desired by satellite users,

Manuscript received June 1, 2021; revised July 18, 2021; accepted July 23, 2021. Date of publication August 12, 2021; date of current version January 17, 2022. This work was supported in part by the National Natural Science Foundation of China under Grant 51827806 and in part by the National Key Research and Development Program of China under Grant 2016YFB0501201. *(Corresponding authors: Fei Xing; Zheng You.)*

Xuedi Chen, Fei Xing, and Zheng You are with the Department of Precision Instrument, Tsinghua University, Beijing 100084, China (e-mail: cxd18@mails.tsinghua.edu.cn; xingfei@mail.tsinghua.edu.cn; yz-dpi@mail.tsinghua.edu.cn).

Xing Zhong is with Chang Guang Satellite Technology Company Ltd., Changchun 130102, China (e-mail: ciomper@163.com).

Kaihua Qi is with the Innovation Academy of Microsatellites, Chinese Academy of Sciences, Shanghai 201204, China (e-mail: 474599085@qq.com).

Digital Object Identifier 10.1109/TGRS.2021.3100841

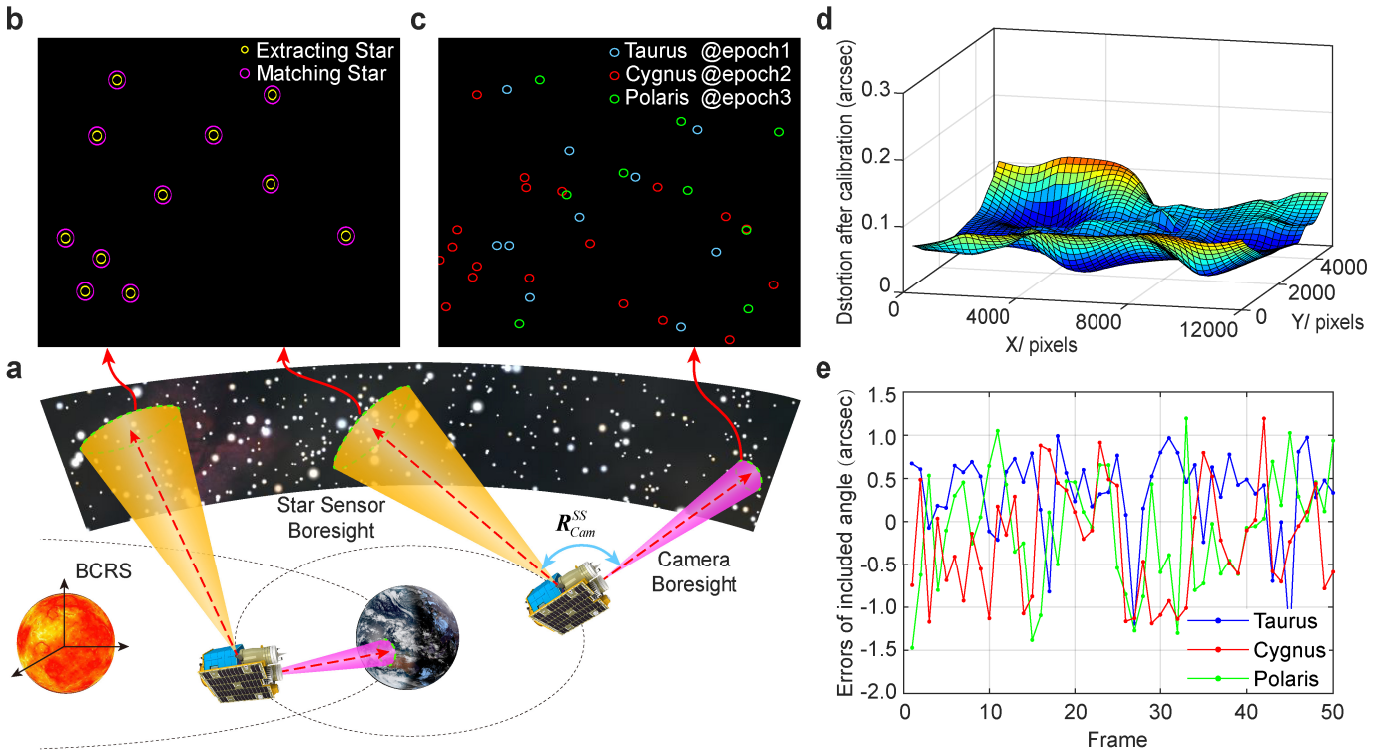

Fig. 1. Diagram of geometric calibration based on star sources observation. (a) On-orbit operation process of Jilin-1 ShiPin07 (JL-1 SP07). (b) Image captured by star sensor and the result of star identification. (c) Superposition of star maps captured by JL-1 SP07 from Taurus, Cygnus, and Polaris at different epochs. (d) Residual distortion after internal calibration. (e) Residual errors of included angle of optical axis after external calibration.

such as Chang Guang Satellite Technology Company Ltd. and the Innovation Academy of Microsatellites. Compared with landmarks, stars can be detected by almost all optical satellites. Moreover, the reference data of stars can be inbuilt into onboard computer easily and the algorithms of extraction and recognition of stars are very mature [22], [23], which guarantees that the star-based method is the best candidate for on-orbit autonomous calibration.

Therefore, the calibration technology based on star control points (SCPs) was proposed and developed. Many meteorological satellites and deep space exploration missions use the stars as the calibration reference. Newburn *et al.* [24] used the star field images for camera geometric calibration in Stardust spacecraft. Guan *et al.* [25] proposed an attitude-independent internal calibration method using star targets to remove the influence of attitude errors and the accuracy of internal calibration could reach 0.3 pixels. Guan *et al.* [21] developed the star-based calibration of external installation matrix between the camera and the star sensor of the Luojia 1-01 satellite, which is a night-light satellite. The bias of external parameters was about 6.2 pixels. However, many studies only focus on either internal calibration or external calibration. Guan *et al.* [21] discussed the external calibration thoroughly. Nevertheless, it did not complete the internal calibration limited by the number of SCPs. Christian *et al.* [17], Wang *et al.* [19], and Guan *et al.* [25] described the internal calibration in detail. Their discussion on external calibration is relatively less.

In this article, we presented an on-orbit geometric calibration method based on star sources observation to calibrate the internal parameters and external installation matrix as a whole. The satellite attitude is adjusted so that both camera and star sensor can capture star sources as SCPs. In order to meet the requirements of number and distribution of control points in internal calibration, star maps from multiregions are captured to obtain enough and evenly distributed SCPs on the image plane. The advantages of the proposed method can be demonstrated in two aspects: 1) compared with landmark-based method, the method can work in special missions where landmarks do not work and has the potential to actualize the on-orbit autonomous geometric calibration for large satellite constellation, and 2) the method captures star sources from different regions at short period as SCPs and realizes the internal and external calibrations simultaneously and accurately.

II. Outline of the Proposed Method

The on-orbit operation of satellite is shown in Fig. 1(a) and divided into calibration stage and remote sensing stage, which is described in the barycentric celestial reference system (BCRS). The coordinate axes of BCRS are consistent with that of the International Celestial Reference System (ICRS). In the remote sensing stage, the camera calibrated by the proposed method conducts the observation mission normally. In the calibration stage, the satellite is controlled so that both the star sensor and the camera can capture the star sources simultaneously. As shown in Fig. 1(b), the star sensor detects the star sources and executes the star identification to calculate the device attitude relative to BCRS. The camera captures and recognizes the star sources the same as star sensor. In order to obtain enough star sources and ensure them to distribute evenly on the full image plane, the camera takes pictures from multiple star regions, as shown in Fig. 1(c). Taking the star sources as control points, we establish the "camera-star sensor"

joint calibration model combining the space–time effects with optical imaging and study the geometric imaging relationship of SCPs through decoupling the influences of relativistic effects and geometric parameters offset. The invariable angular distance between SCPs in camera is used as a constraint to calibrate the internal parameters, including focal length and distortion. The average residual distortion of internal calibration is below 0.1", as shown in Fig. 1(d). The geometric relationship between camera and star sensor is used to estimate the external installation matrix of camera. The included angle of optical axis between camera and star sensor is applied to evaluate the accuracy of external calibration because it is constant in a short period. As shown in Fig. 1(e), the error of external calibration is within ± 1.4".

Compared with the traditional method established upon ground calibration sites, the method based on star sources observation should study the deviation between the apparent directions and the standard directions of star sources, which are stored in star catalog. The deviation mainly includes four parts: proper motion, parallax, stellar aberration, and gravitational deflection [26], [27]. The proper motion and parallax are about the order of subarcsecond, which is close to the order of single-pixel angular resolution of remote sensing camera. Therefore, they should be considered for internal calibration. The latter two need to be explained in the relativity framework. The stellar aberration effect is relative to the motion state of satellite. As for the satellite in low Earth orbit (LEO), the maximum deviation angle brought from stellar aberration is up to 26", which cannot be ignored. The perturbation from gravitational deflection of star light is small (microarcseconds to a few milliarcseconds) so that the cameras cannot detect it. In order to compensate for the deviation, we should establish the star observation model (SOM) to compensate for the deviation stemmed from space–time effects, including proper motion, parallax, and stellar aberration.

The "camera-star sensor" joint calibration model is used to decouple space–time effects and bias of geometric parameters in star sources imaging and actualize the geometric calibration, which includes three main parts.

First, after star extraction and recognition, the SOM is set to compensate for deviations caused by proper motion, parallax, and stellar aberration, which are sensitive to satellite ephemeris, including observation time (t), satellite position ($\boldsymbol{r}_{\text{sat}}$), and velocity ($\boldsymbol{v}_{\text{sat}}$) in BCRS. The SOM can be formulated succinctly as follows:

$$\boldsymbol{u}_{i,\text{ob}}(t) = f(\boldsymbol{u}_i|t, \boldsymbol{r}_{\text{sat}}(t), \boldsymbol{v}_{\text{sat}}(t)) \tag{1}$$

where $\boldsymbol{u}_{i,\text{ob}}(t)$ is the apparent direction of star i relative to satellite as the calibration reference and $\boldsymbol{u}_i$ is the standard direction of star i in the star catalog.

Then, the geometric relationship of star sources in camera is established for the internal calibration. The principle of calibration can be represented briefly

$$\min_{\boldsymbol{X}_I} \sum_{i=1}^{n-1} \sum_{j=i+1}^{n} \left\| \left(\boldsymbol{u}_{i,\text{ob}}(t)\right)^T \boldsymbol{u}_{j,\text{ob}}(t) - \left(\boldsymbol{w}_i(\boldsymbol{X}_I)\right)^T \boldsymbol{w}_j(\boldsymbol{X}_I) \right\|_2 \tag{2}$$

where $\boldsymbol{X}_I$ is the aggregation of internal parameters, including the focal length and distortion, $\boldsymbol{w}_i$ is the unit vector of star i measured in the camera coordinate system, and n is the number of SCPs.

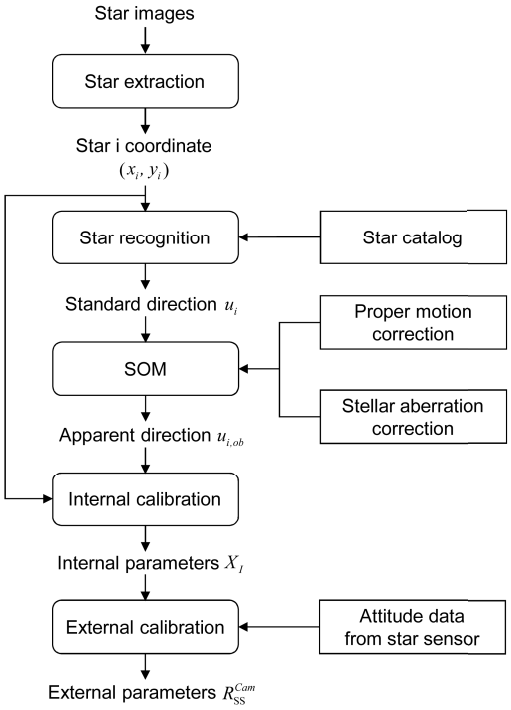

Fig. 2. Procedures of on-orbit autonomous calibration based on star sources observation.

Finally, on the basis of internal parameters calibrated and installation relationship between camera and star sensor, the external installation matrix of camera is estimated. Finally, the high-accuracy geometric calibration is completed.

Fig. 2 shows the procedures of the geometric calibration based on star sources observation and each step can be implemented autonomously in the onboard computers. The algorithms of star extraction and recognition are very mature and the SOM given by (1) can also easily conducted, which will be explained thoroughly in Section III. The estimation of aggregates of the internal parameters $\boldsymbol{X}_I$ and the external parameters $\boldsymbol{R}_{\text{Cam}}^{\text{SS}}$ is based on the optimization iteration method and there is a certain amount of calculation in this process, which may be the obstacle to autonomous geometric calibration. Actually, it is not necessary to accomplish calibration immediately after capturing the star images. We can complete the calculation when the satellite is in the spare time. Therefore, the method based on stars is fully capable of fulfilling the requirements of autonomous calibration proposed by some satellite users, such as Chang Guang Satellite Technology Company Ltd and the Innovation Academy of Microsatellites.

III. "Camera-Star Sensor" Joint Calibration Model

The "camera-star sensor" joint calibration model describes the imaging geometric relationships of apparent direction of star sources in camera and between camera and star sensor, as shown in Fig. 3, which integrates the space–time effects and optical imaging in star sources observation. The model decouples precisely the influences of relativistic effects and

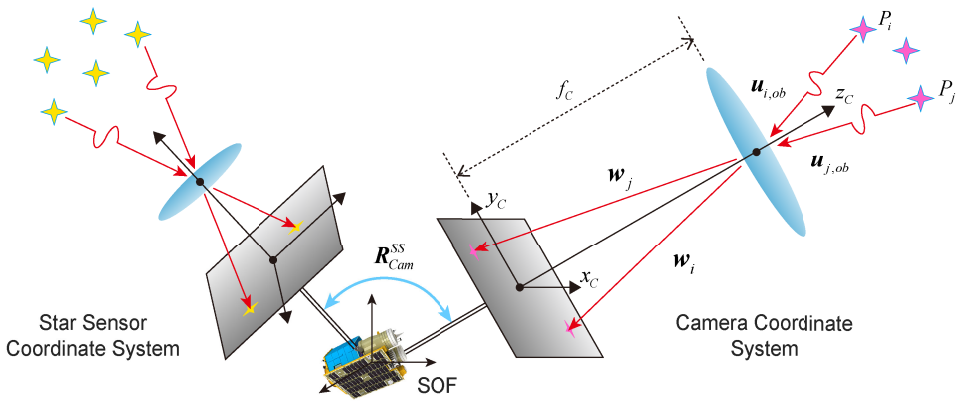

Fig. 3. Diagram of "camera-star sensor" joint calibration model.

the distortion of geometric parameters and includes three parts as in Section II.

A. Star Observation Model

The standard directions of star sources in star catalog are defined in the BCRS at the standard epoch and are in the absence of special relativistic perturbations. They are different from the apparent directions of star sources observed by satellites at arbitrary epoch, which are the real calibration control points. We represent the satellite observation frame (SOF) to define the apparent directions, whose origin of SOF is the satellite barycenter and axes are consistent with that of BCRS. The SOM is established to compensate for the deviation of apparent directions, which includes proper motion, parallax, and stellar aberration. The proper motion and parallax represent the influence caused by the motion of star sources and the satellite, which can be explained in the classical Newtonian framework. The stellar aberration is the perturbation due to the relative motion between the SOF and the BCRS.

1) Proper Motion and Parallax: Modern star catalogs store astrometric data of star sources, including the data of standard position, proper motion, and parallax. Our proposed calibration method assumes the use of Tycho-2 catalog, which is the most widely used photographic reference catalog. To ensure consistency with Tycho-2 catalog, the SOM adopts the "standard model" for correcting the deviation caused by proper motion and parallax, whose premise assumption is that all star sources move at a uniform velocity relative to the solar-system barycenter [28]. There are six astrometric parameters recorded in star catalog for describing the motion of star sources. The six astrometric parameters are: 1) α_i, the right ascension of star i in BCRS at standard epoch t_{ep}; 2) δ_i, the declination of star i in BCRS at t_{ep}; 3) $\mu_{\alpha i}$, the velocity of proper motion in right ascension; 4) $\mu_{\delta i}$, the velocity of proper motion of declination; 5) μ_{ri}, the velocity of radical proper motion; and 6) ϖ_i, the annual parallax of star i. According to the above parameters, the standard direction of star i defined in BCRS at t_{ep} is given by

$$\boldsymbol{u}_i = \begin{bmatrix} \cos(\delta_i)\cos(\alpha_i) \\ \cos(\delta_i)\sin(\alpha_i) \\ \sin(\delta_i) \end{bmatrix}. \tag{3}$$

Under the assumption that every star source moves at uniform velocity, the star direction $\boldsymbol{u}_i'(t)$ relative to a fictitious stationary observer at the origin of SOF at arbitrary time t is derived from the "standard model"

$$\boldsymbol{u}_i'(t) = \left\langle \boldsymbol{u}_i + \left[t_B - t_{\text{ep}}\right]\left(\mu_{\alpha i}\boldsymbol{p}_i + \mu_{\delta i}\boldsymbol{q}_i + \mu_{ri}\boldsymbol{u}_i\right) - \varpi_i \boldsymbol{r}_{\text{sat}}(t)/\text{Au}\right\rangle. \tag{4}$$

The triangular brackets $\langle\cdot\rangle$ represent the normalization of vector. Au is the astronomical unit. The triad $\{\boldsymbol{p}_i, \boldsymbol{q}_i, \boldsymbol{u}_i\}$ forms a ternary orthogonal basis, whose directions are the increasing direction of right ascension and declination and the radial direction relative to the solar-system barycenter. Therefore, $\boldsymbol{p}_i = \langle \boldsymbol{z} \times \boldsymbol{u}_i \rangle$ and $\boldsymbol{q}_i = \boldsymbol{u}_i \times \boldsymbol{p}_i$, where $\boldsymbol{z} = [0, 0, 1]^T$. The effect of radical proper motion can be ignored by setting $\mu_{ri} = 0$ for nearly all star sources. t_B expresses the observation time after correcting the Römer delay [29], which is given by $t_B = t + \boldsymbol{u}_i^T \boldsymbol{r}_{\text{sat}}(t)/c$, where c denotes the velocity of light. Thus, the Römer delay is up to 500 s at most for LEO satellite. Assuming that the satellite observes Barnard, whose proper motion is the fastest and reaches about 10.3"/year, the deviation caused by the Römer delay is up to 0.163 mas, which cannot be detected by a remote sensing camera.

Therefore, (4) can be safely simplified in most cases, leading to

$$\boldsymbol{u}_i'(t) = \left\langle \boldsymbol{u}_i + \left[t - t_{\text{ep}}\right]\left(\mu_{\alpha i}\boldsymbol{p}_i + \mu_{\delta i}\boldsymbol{q}_i\right) - \varpi_i \boldsymbol{r}_{\text{sat}}(t)/\text{Au}\right\rangle. \tag{5}$$

2) Stellar Aberration: Stellar aberration denotes the phenomenon that the direction of light source observed by the moving observer differs from that observed by the stationary observer at the same place. It is the result of the superposition of velocity under the theory of special relativity [26], [27], [30]. The stellar aberration effect involved in this article is the deviation between the apparent direction $\boldsymbol{u}_{i,\text{ob}}$ of star i in SOF at observation time and the star direction $\boldsymbol{u}_i'$ observed by a fictitious stationary observer at satellite barycenter at observation time, which is caused by the relative motion between SOF and BCRS. Under the theory of special relativity, the transformation between the apparent direction $\boldsymbol{u}_{i,\text{ob}}$ and the star direction $\boldsymbol{u}_i'$ follows the Lorentz transformation and the Lorentz factor is introduced as

$$\gamma = 1/\sqrt{1 - \boldsymbol{\beta}^T\boldsymbol{\beta}} \tag{6}$$

where $\boldsymbol{\beta} = \boldsymbol{v}_{\text{sat}}/c$. According to the Lorentz transformation, the reference apparent direction $\boldsymbol{u}_{i,\text{ob}}$ can be derived as

$$\boldsymbol{u}_{i,\text{ob}} = \left(1+\boldsymbol{\beta}^T\boldsymbol{u}_i'\right)^{-1}\left[\boldsymbol{u}_i'+\left(1-\gamma^{-1}\right)\langle\boldsymbol{\beta}\rangle\times\left(\langle\boldsymbol{\beta}\rangle\times\boldsymbol{u}_i'\right)+\boldsymbol{\beta}\right]. \tag{7}$$

As for the satellite observer, $\boldsymbol{v}_{\text{sat}}$ expresses the satellite velocity in BCRS, which means that it is the superposition of the satellite orbital velocity $\boldsymbol{v}_{\text{orbit}}$ in the Earth-centered inertial (ECI) frame and the Earth's revolution velocity $\boldsymbol{v}_{\text{earth}}$ in BCRS. The orbital velocity generally measured by GPS is about 8 km/s for the LEO satellite. The Earth's revolution velocity estimated from the observation time is about 30 km/s [31]. The maximum velocity of the LEO satellite can reach 38 km/s. Therefore, $\|\boldsymbol{\beta}\|$ is approximately equal to 10^{-4} and it is reasonable to consider $\boldsymbol{\beta} \to 0_{3\times1}$ and $\gamma \to 1$. After the Taylor expansion of term $\left(1+\boldsymbol{\beta}^T\boldsymbol{u}_i'\right)^{-1}$ and $\left(1-\gamma^{-1}\right)$, (7) can be expanded as follows:

$$\begin{aligned}\boldsymbol{u}_{i,\text{ob}} = {} & \boldsymbol{u}_i' \\ & + \left[\boldsymbol{u}_i'\times\left(\boldsymbol{\beta}\times\boldsymbol{u}_i'\right)\right] \\ & - \left[\left(\boldsymbol{\beta}^T\boldsymbol{u}_i'\right)\boldsymbol{u}_i'\times\left(\boldsymbol{\beta}\times\boldsymbol{u}_i'\right)+\frac{1}{2}\boldsymbol{\beta}\times\left(\boldsymbol{u}_i'\times\boldsymbol{\beta}\right)\right] \\ & + \left[\left(\boldsymbol{\beta}^T\boldsymbol{u}_i'\right)^2\boldsymbol{u}_i'\times\left(\boldsymbol{\beta}\times\boldsymbol{u}_i'\right)+\frac{1}{2}\left(\boldsymbol{\beta}^T\boldsymbol{u}_i'\right)\boldsymbol{\beta}\times\left(\boldsymbol{u}_i'\times\boldsymbol{\beta}\right)\right] \\ & + o\left(c^{-4}\right).\end{aligned} \tag{8}$$

Assume that the satellite velocity is about 38 km/s, the first-order of stellar aberration reaches 26.1", the second order of effect is up to 4.7×10^{-3}", and the third-order may amount to 1×10^{-6}". Generally, the resolution of remote sensing camera can reach the order of subarcsecond. Consequently, it is reasonable to consider only the first order of stellar aberration and simplify (8) as follows:

$$\boldsymbol{u}_{i,\text{ob}} = \left\langle\boldsymbol{u}_i'+\left[\boldsymbol{u}_i'\times\left(\boldsymbol{\beta}\times\boldsymbol{u}_i'\right)\right]\right\rangle = \left\langle\left(\boldsymbol{I}_{3\times3}-[\boldsymbol{\delta}_a\times]\right)\boldsymbol{u}_i'\right\rangle \tag{9}$$

where $\boldsymbol{\delta}_a = \boldsymbol{u}_i'\times\boldsymbol{\beta}$ and the bracket $[\cdot\times]$ denotes the antisymmetric matrix.

B. Internal Calibration Model

To avoid the influence of attitude error, an attitude-independent method of calibrating the internal parameters (focal length and distortion) is proposed. The foundation of attitude-independent calibration method is that the corresponding star angular distance is invariant whether in the camera coordinate system or in the SOF. It is worth noting that the invariance of star angular distance is not suitable between the camera coordinate system and the BCRS because of the proper motion, parallax, and stellar aberration. Consequently, the invariance is given by

$$\cos\left(\theta_{ij}\right) = \boldsymbol{u}_{i,\text{ob}}^T\boldsymbol{u}_{j,\text{ob}} = \boldsymbol{w}_i^T\boldsymbol{w}_j \tag{10}$$

where θ_{ij} is the angle of two star vectors and $\boldsymbol{w}_i$ denotes the measured unit vector of star P_i measured in camera coordinate with internal parameter error expressed as follows:

$$\begin{aligned}\boldsymbol{w}_i &= \begin{bmatrix}X_i\\Y_i\\Z_i\end{bmatrix} \\ &= \frac{1}{\sqrt{\left(x_i-x_0-x_{i,d}\right)^2+\left(y_i-y_0-y_{i,d}\right)^2+\left(f_c-\Delta f\right)^2}} \\ &\quad\times\begin{bmatrix}x_i-x_0-x_{i,d}\\y_i-y_0-y_{i,d}\\-\left(f_c-\Delta f\right)\end{bmatrix}\end{aligned} \tag{11}$$

where (x_i, y_i) denotes the coordinate position of star i on the image. The coordinates (x_0, y_0) are the principal point and f_c is the focal length. However, due to the imperfection of optical system, the internal parameters will be deviated. The deviation includes the focal length error Δf and the synthetic distortion $\left(x_{i,d}, y_{i,d}\right)$ consisting of optical lens distortion and principal point offset. The distortion error relates to the principal point offset $(\Delta x_0, \Delta y_0)$, the radial distortion (k_1, k_2), and the decentering distortion (p_1, p_2) represented by

$$\begin{cases}x_{i,d} = \bar{x}\left(q_1l^2+q_2l^4\right)+\left[p_1\left(l^2+2\bar{x}^2\right)+2p_2\bar{x}\bar{y}\right]+\Delta x_0\\ y_{i,d} = \bar{y}\left(q_1l^2+q_2l^4\right)+\left[p_2\left(l^2+2\bar{y}^2\right)+2p_1\bar{x}\bar{y}\right]+\Delta y_0\end{cases} \tag{12}$$

where $\bar{x} = x_i - x_0$, $\bar{y} = y_i - y_0$, and $l = \sqrt{\bar{x}^2+\bar{y}^2}$. The calibration model is not practical because of the overparameterization and the strong correlation among some parameters in some cases. Therefore, the aggregate of internal parameter error includes the focal length error and the distortion error, $\boldsymbol{X}_I = \left(f_C, x_{1,d}, y_{1,d}, \ldots, x_{n,d}, y_{n,d}\right)^T$. n denotes the number of SCPs.

To suppress the influence of random error in star point extraction, the SCPs from multiframe star images of the same star region are used for internal calibration. After calibration, the synthetic distortion value of each SCP can be obtained, which should be expanded into a distortion model of full image plane. The thin-plate spline is utilized to expand the model, which has the potential to remove complex distortions [32].

C. External Calibration Model

The external installation matrix between camera and star sensor is important for image position determination. However, there is a deviation caused by stellar aberration in star sources observation. Taking the stars for the celestial navigation, the deviation brings the attitude error into the results outputted by the attitude determination device. Because of its sensitivity to velocity of satellite relative to BCRS, the attitude error is inconsistent at each moment. Thus, the external parameters also keep changing over time.

To decouple the deviation in external calibration, we established the external calibration model based on the influence of stellar aberration and the geometric relationship between camera and star sensor. The external calibration model can be represented by

$$\boldsymbol{w}_i(t) = \boldsymbol{u}_{i,\text{ob}}^C(t) = \lambda\boldsymbol{R}_{\text{SS}}^{\text{Cam}}(\boldsymbol{X}_E)\boldsymbol{R}_{\text{corr}}(\boldsymbol{\delta}_{\text{ss}})\boldsymbol{R}_{\text{BCRS}}^{\text{SS}}(t)\boldsymbol{u}_{i,\text{ob}}(t) \tag{13}$$

where λ is the proportional coefficient and $\boldsymbol{u}_{i,\mathrm{ob}}^{C}(t)$ is the theoretical imaging vector of star i in the camera coordinate system at the time t, which should be consistent with $\boldsymbol{w}_i(t)$ in theory. $\boldsymbol{R}_{\mathrm{BCRS}}^{\mathrm{SS}}(t)$ is the attitude matrix from BCRS to star sensor coordinate system expanded by the quaternion (q_1, q_2, q_3, q_4) of star sensor at time t and q_4 is the scalar. However, the navigation benchmark built into star sensor is generally the standard direction of star sources in the absence of perturbation from stellar aberration. It is reasonable to correct the attitude data from star sensor. However, it is not appropriate to rectify the attitude matrix from star sensor by extending (9) directly, which is suitable for correction of star direction vectors. According to the geometric meaning of the cross product in (9), the transformation relation of attitude matrix can be represented by using the axis/angle formula. The axis is the unit vector parallel to $\boldsymbol{\delta}_{\mathrm{SS}} = \boldsymbol{z}_{\mathrm{bore}} \times \boldsymbol{\beta}$ and the sine of rotation angle is the norm of $\boldsymbol{\delta}_{\mathrm{SS}}$, where $\boldsymbol{z}_{\mathrm{bore}}$ denotes a unit vector aligned with boresight of star sensor composed of the three elements in the last row of $\boldsymbol{R}_{\mathrm{BCRS}}^{\mathrm{SS}}(t)$. Therefore, the correct quaternion can be represented by

$$(\Delta q_1, \Delta q_2, \Delta q_3, \Delta q_4) = (\boldsymbol{\delta}_{\mathrm{SS}}/2, 1 - \langle \boldsymbol{\delta}_{\mathrm{SS}}/2 \rangle) \tag{14}$$

where $\boldsymbol{\delta}_{\mathrm{SS}} = \boldsymbol{z}_{\mathrm{bore}} \times \boldsymbol{\beta}$ and $\boldsymbol{z}_{\mathrm{bore}}$ denotes a unit vector aligned with boresight of star sensor composed of the three elements in the last row of $\boldsymbol{R}_{\mathrm{BCRS}}^{\mathrm{SS}}(t)$. The correct matrix $\boldsymbol{R}_{\mathrm{corr}}(\boldsymbol{\delta}_{\mathrm{ss}})$ can be derived by the correct quaternion. $\boldsymbol{R}_{\mathrm{SS}}^{\mathrm{Cam}}(\boldsymbol{X}_E)$ is the external installation matrix from camera to star sensor, which should be calibrated and is expressed as follows:

$$\boldsymbol{R}_{\mathrm{SS}}^{\mathrm{Cam}}(\boldsymbol{X}_E) = \begin{bmatrix} a_1 & b_1 & c_1 \\ a_2 & b_2 & c_2 \\ a_3 & b_3 & c_3 \end{bmatrix} \tag{15}$$

the aggregate of external parameters including nine elements, $\boldsymbol{X}_E = (a_1, a_2, a_3, b_1, b_2, b_3, c_1, c_2, c_3)^T$.

IV. Estimation Method of Geometric Parameters

The calibration model is introduced in Section III for estimating the aggregate of internal parameters $\boldsymbol{X}_I$ and the aggregate of external parameters $\boldsymbol{X}_E$. The calibration algorithm is the optimization iteration method based on the least-square theory. The internal parameters are calculated at first according to the invariance of star angular distance. Then, the external parameters calibration process is established with the corrected internal parameters and the imaging model between camera and star sensor.

A. Estimation of the Internal Parameters

After star recognition and the correction of SOM, we obtain the reference apparent direction of star sources and the star vectors measured in the camera coordinate system. Assuming that the number of SCPs in an image frame is n and the initial values of distortion errors are zero, the focal length is initialized with the result via on-ground calibration. The initial internal parameters are represented by $\boldsymbol{X}_I^0 = [0, \ldots, 0, f_c]^T$. Then, the residual error equation in the kth iteration can be set according to the least-square theory as follows:

$$r_{ij}^k = \boldsymbol{u}_{i,\mathrm{ob}}^T \boldsymbol{u}_{j,\mathrm{ob}} - \boldsymbol{w}_i^T\left(\boldsymbol{X}_I^k\right)\boldsymbol{w}_j\left(\boldsymbol{X}_I^k\right) = \boldsymbol{u}_{i,\mathrm{ob}}^T \boldsymbol{u}_{j,\mathrm{ob}} - F_{ij}\left(\boldsymbol{X}_I^k\right). \tag{16}$$

Equation (16) can be represented by linearizing

$$r_{ij}^k = \begin{bmatrix} \dfrac{\partial F_{ij}^k}{\partial x_{1,d}} & \dfrac{\partial F_{ij}^k}{\partial y_{1,d}} & \cdots & \dfrac{\partial F_{ij}^k}{\partial x_{i,d}} & \dfrac{\partial F_{ij}^k}{\partial y_{i,d}} & \cdots & \dfrac{\partial F_{ij}^k}{\partial x_{n,d}} & \dfrac{\partial F_{ij}^k}{\partial y_{n,d}} & \dfrac{\partial F_{ij}^k}{\partial f_c} \end{bmatrix} \Delta \boldsymbol{X}_I^k \tag{17}$$

where r_{ij}^k denotes the angular distance residual error equation between star i and j in the kth iteration, $i = 1, 2, \ldots, n-1$, and $j = i+1, i+2, \ldots, n$.

As for one image frame, (17) can be expanded as

$$\boldsymbol{R}^k = \boldsymbol{A}^k \Delta \boldsymbol{X}_I^k \tag{18}$$

where $\boldsymbol{R}^k$ is the residual vector of angle distance between SCPs calculated by the internal parameters in the kth iteration, $\boldsymbol{A}^k$ denotes the Jacobian matrix of internal parameters after linearization, and $\Delta \boldsymbol{X}_I^k$ represents the correction vector of internal parameters in the kth iteration.

According to the least-square theory, the correction vector of internal parameters in the kth iteration can be derived as follows:

$$\Delta \boldsymbol{X}_I^k = \left[\left(\boldsymbol{A}^k\right)^T \boldsymbol{A}^k\right]^{-1} \boldsymbol{A}^k \boldsymbol{R}^k. \tag{19}$$

Then, the internal parameters can be updated after each iteration until the module of correction vector is less than a small positive number.

B. Estimation of the External Parameters

After calibrating the internal parameters, the precise imaging model of camera is obtained and the external parameters can be calibrated with the attitude data from the star sensor. The calibration model of external parameters is represented as (13), and the external parameters are initialized with the on-ground calibration result $\boldsymbol{X}_E^0$. The residual error equation of SCP in the kth iteration can be rewritten by (13) as follows:

$$\boldsymbol{E}_i^k = \begin{bmatrix} L_i^k \\ M_i^k \end{bmatrix} = \begin{bmatrix} \dfrac{a_1^k U_{i,x} + b_1^k U_{i,y} + c_1^k U_{i,z}}{a_3^k U_{i,x} + b_3^k U_{i,y} + c_3^k U_{i,z}} - \dfrac{X_i}{Z_i} \\ \dfrac{a_2^k U_{i,x} + b_2^k U_{i,y} + c_2^k U_{i,z}}{a_3^k U_{i,x} + b_3^k U_{i,y} + c_3^k U_{i,z}} - \dfrac{Y_i}{Z_i} \end{bmatrix} \tag{20}$$

where

$$\begin{bmatrix} U_{i,x} \\ U_{i,y} \\ U_{i,z} \end{bmatrix} = \boldsymbol{R}_{\mathrm{corr}}(\boldsymbol{\delta}_{\mathrm{ss}}) \boldsymbol{R}_{\mathrm{BCRS}}^{\mathrm{SS}}(t) \boldsymbol{u}_{i,\mathrm{ob}}(t). \tag{21}$$

The residual error equation of SCP in the kth iteration can be linearized leading to

$$\boldsymbol{E}_i^k = \boldsymbol{B}_i^k \Delta \boldsymbol{X}_E^k \tag{22}$$

where $\boldsymbol{E}_i^k$ is the residual vector of SCP in the kth iteration, n is the number of SCPs, $i = 1, \ldots, n$, $\boldsymbol{B}_i^k$ denotes the Jacobian matrix of external parameters in the kth iteration, and $\Delta \boldsymbol{X}_E^k$ is the correction vector of external parameters in the kth iteration. Equation (22) can be expanded by all SCPs in single image frame and the correction vector of external parameters can be obtained according to the least-square method as follows:

$$\Delta \boldsymbol{X}_E^k = \left[\left(\boldsymbol{B}^k\right)^T \boldsymbol{B}^k\right]^{-1} \boldsymbol{B}^k \boldsymbol{E}^k \tag{23}$$

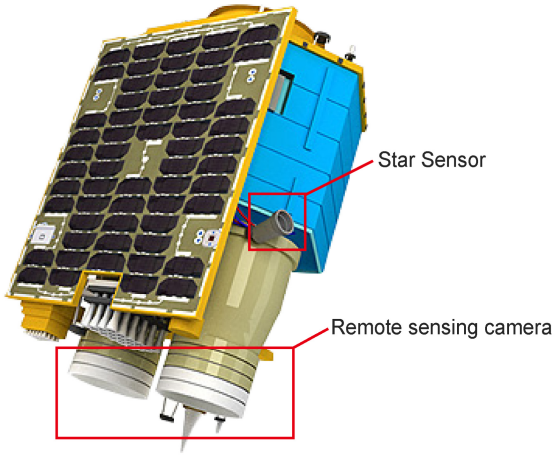

Fig. 4. Physic picture of JL-1 SP07 with camera and star sensor.

where $\boldsymbol{B}^k = \left(\boldsymbol{B}_i^k\right)^T$ and $\boldsymbol{E}^k = \left(\boldsymbol{E}_i^k\right)^T$, $i = 1, \ldots, n$. Then, the external parameters can be updated after each iteration according to the results calculated by (23). The update process will be stopped when the module of correction vector is less than a small positive number.

V. Experiments and Discussion

A. Dataset

An on-orbit calibration experiment was carried out on JL-1 SP07, which was a high remote sensing satellite launched by Chang Guang Satellite Technology Company Ltd. on January 19, 2018. It was in a 535-km sun-synchronous solar orbit with a 97.54° inclination. The satellite was equipped with a remote sensing camera and high-accuracy star sensors, which were used to verify the performance of the proposed method. The physic picture of JL-1 SP07 with camera and star sensor is shown in Fig. 4. The star sensor onboard is the NST4S-A2 star tracker manufactured by TY-Space Technology (Beijing) Ltd. The NST4S-A2 star tracker is characterized by excellent dynamic performance, high update rate, and high precision. The GPS was used to obtain the velocity and position of satellite, which is related to the space–time effects. The detailed information of payload and star sensors onboard is listed in Tables I and II, respectively.

In the process of experiment, the satellite attitude was controlled to guarantee both remote sensing camera and star sensor can detect the star sources as SCPs. Because of the large aperture of camera, the ability to detect weak star sources is remarkable so that the camera can capture the star with about 12 magnitudes. Therefore, the Tycho-2 catalog is used as the initial measurement benchmark in this article, which stores the accurate astrometric data of about 250 million star sources [33]. We captured 50 star images from Taurus, Cygnus, and Polaris regions as test data. The several frame data of SCPs were used to suppress the influence of random error in the calibration. A description of star regions is listed in Table III. To obtain the SCPs from star images, we conducted the star identification with the Tycho-2 catalog. There are about 22 SCPs from the Taurus region, 54 SCPs from the Cygnus region, and 15 SCPs from the Polaris region.

TABLE I
Parameters of the Remote Sensing Camera on JL-1 SP07

Characteristics	Value
Focal length(mm)	3220mm
The resolution of detector(pixel)	12000(W) × 5000(W)
The size of pixel(mm)	0.0055mm
FOV(degree)	1.17° × 0.49°
Angular resolution(arcsecond)	0.35″

TABLE II
Parameters of the Star Sensor on JL-1 SP07

Characteristics	Value
Pointing Accuracy(arcsecond)	< 3″(3σ)
Update rate(Hz)	10Hz
Dynamical performance(°/s)	3°/s
FOV(degree)	1.5° × 18°

B. Internal Calibration Result and Accuracy Assessment

Based on the SCPs obtained from star images, the internal calibration was conducted. In order to avoid the influence of the attitude error, we used the invariable star angular distance relationship between SCPs in the camera imaging coordinate system as geometric constraint, which realized the attitude-independent internal calibration.

The full coverage of the SCPs on the image plane is the key to ensuring the global optimization of the internal calibration. However, it is difficult to meet the coverage requirements by capturing SCPs from a single star region. Fig. 5(a) shows the distribution of all SCPs from three star regions on the image plane. The green points denote the SCPs captured from the Polaris region. From Fig. 5(a), we can see that the number of green points is relatively small and most of them are located at the edge of the image plane. In a short period of time, the internal parameters of camera are constant. Therefore, it is reasonable to think that the internal parameters are consistent during the shooting of three regions and use all SCPs from three regions to conduct the internal calibration. As shown in Fig. 5(a), the SCPs basically cover the entire image plane.

Another factor that affects the internal calibration accuracy is the star extraction error. The star extraction error is inevitable and the magnitude of it is about 0.1 pixel. In order to suppress the influences of star extraction, we adopted multiframe star images for internal calibration in JL-1 SP07 and the final results are the average of the values obtained from multiple frames.

To verify the performance of the proposed method, the first 40 frames in the 50 frames star images were used as the calibration frames and the 10 frames were applied as the accuracy assess frames. According to the camera attitude calculated by star identification, the apparent directions of SCPs were reversed to the theoretical imaging vector of SCPs in the camera coordinate system. Due to the distortion of internal parameters, there were deviations between the theoretical imaging vectors and the measured vectors of SCPs. Fig. 5(b) shows the distribution of the average residual errors of all SCPs on the image plane in accuracy access frames. After the

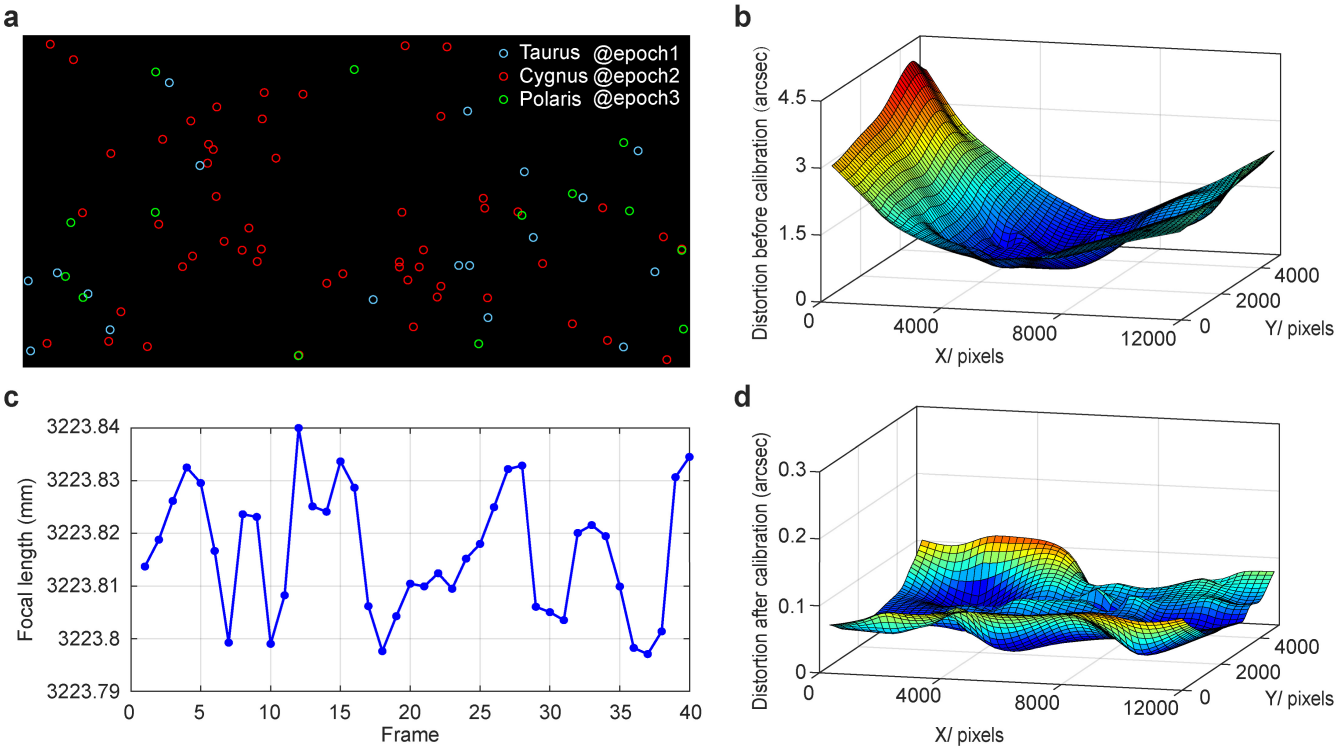

Fig. 5. (a) Distribution of SCPs captured from three star regions by JL-1 SP07 at different epochs. (b) Residual distortion before internal calibration. (c) Calibration results of focal length calculated by 40 calibration frames. (d) Residual distortion after internal calibration.

TABLE III
INFORMATION OF STAR IMAGES

Star region	Start epoch of imaging	Center position	Number of SCPs
Taurus	UTC 2020.04.07 22:11:06	(03h45m14.06s, 23°23′24.36″)	22
Cygnus	UTC 2020.04.07 23:48:38	(20h11m27.91s, 36°01′06.24″)	54
Polaris	UTC 2020.04.07 17:16:55	(03h10m36.82s, 88°57′30.60″)	15

TABLE IV
EXTERNAL CALIBRATION RESULTS IN QUATERNION FORM

Star region	q_1	q_2	q_3	q_4
Taurus	0.707404523041756	0.487032534504335	-0.285681598699700	0.425163705192133
Cygnus	0.707453494632808	0.486957924783494	-0.285704543054475	0.425152274364593
Polaris	0.707388352644178	0.487055279854537	-0.285771586968112	0.425104088170814

estimation of internal parameters based on the 40 calibration frames, the results of focal length are shown in Fig. 5(c). The focal length calibrated can be obtained by averaging the results of 40 frames and was 3223.816 mm. The accuracy of focal length was about 12 μm. As for the calibration of synthetic distortion, we could estimate the distortion value of each SCP and average the distortion values calculated by 40 calibration frames as the calibration results. In accuracy assess frames, the results of internal parameters were reversed to get the measured vectors of SCPs calibrated. The distribution of average residual errors of all SCPs after calibration is shown in Fig. 5(d). The average residual errors were reduced from about 4" to less than 0.1".

The root mean square (rms) of residual errors between the theoretical imaging vectors and the measured vectors of SCPs calibrated was used to assess the accuracy of internal calibration, which was given by

$$\mathrm{RMS}_I = \sqrt{\frac{\sum_{i=1}^{n}(\arccos(\boldsymbol{W}_i^T \boldsymbol{u}_{i,\mathrm{ob}}^C))^2}{n}} \tag{24}$$

where n is the number of SCPs and $\boldsymbol{u}_{i,\mathrm{ob}}^C$ is the theoretical imaging vectors of SCPs calculated by (13). The accuracy of the internal calibration was 0.052" or about 0.15 pixels according to the angular resolution of single pixel, which illustrated the effectiveness of the proposed method.

C. External Calibration Result and Accuracy Assessment

Different from the internal calibration, the external calibration of installation matrix between camera and star sensor does not need to integrate all SCPs from three star regions. The SCPs from single star region can be used to complete

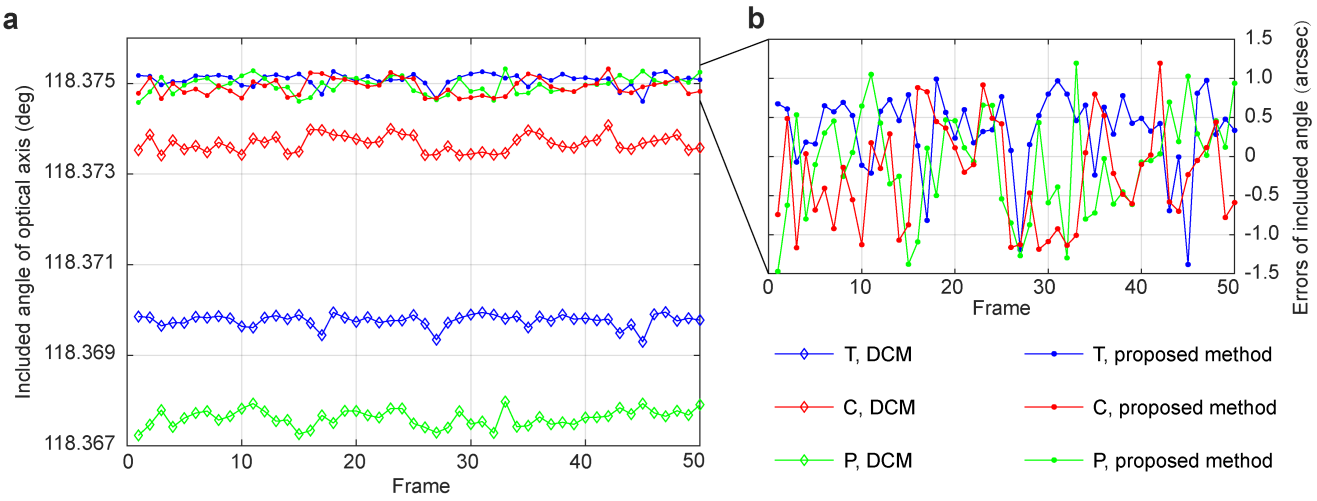

Fig. 6. (a) Included angles of optical axis between camera and star sensor calibrated by the DCM and the proposed method respectively. (b) Residual errors of included angles calculated by the proposed method. T, C, and P denote Taurus, Cygnus, and Polaris, respectively.

the external calibration. According to the external calibration model represented by (13) and the estimated method, the external parameters can be calculated. In order to express the result conveniently, the external installation matrix is expressed in the form of quaternion instead of cosine matrix. The calibration results from three star regions are shown in Table IV, where q_4 is the scalar.

The calibration results of the proposed method were compared with those of direct calibration method (DCM), which was mentioned in many papers. The DCM directly applied the attitude data outputted by star sensor and the imaging information of control points. Then, the imaging geometric model of SCPs was established, based on which an iterative method was used to implement the external calibration.

The attitude cosine matrix and quaternion cannot intuitively express the calibration accuracy of external parameters. We utilized the included angle of optical axis between camera and star sensor to evaluate the method accuracy because it is constant basically in short period of time. In this experiment, the maximum time interval among the imaging epochs was about 6 h. Therefore, it was reasonable to think that the included angle of optical axis was consistent in the process of imaging. Fig. 6(a) shows the included angles of optical axis calibrated by the DCM and the proposed method. We could see that the maximum deviation of included angle calculated by DCM was up to 21.6". For JL-1 SP07 who conducted the experiments, the deviation could cause about 50-m positioning error at the process of Earth observation, which is unacceptable. The great deviation was mainly because the DCM did not consider the influence of stellar aberration. As for the proposed method, the included angle calibrated from three star regions was consistent with each other basically. In order to further illustrate the calibration accuracy of external parameters with this method, the residual errors of included angle of optical axis between camera and star sensor are shown in Fig. 6(b). It is worth noting that the external calibration mainly eliminates the systematic bias in the installation matrix. The rms of included angles mainly contains the attitude error of star sensor. Consequently, the range of included angles is used to assess the accuracy of the calibration method. It is clear that the error of the external installation matrix is within ± 1.4", which can demonstrate the superiority and effectiveness of the proposed method.

VI. Conclusion

Our purpose of the geometric calibration method based on star sources observation is to actualize the high-accuracy autonomous calibration of internal parameters and external installation matrix even when the availability of landmarks is hard. Combining with the space–time effects and optical imaging in star sources observation, the "camera-star sensor" joint calibration model is established for geometric calibration. As the on-orbit experiment results shown, the internal calibration eliminates the imaging distortion providing the precise mapping relationships between the imaging points and the apparent directions of targets in inertial space. The external calibration compensates for the systematic error in the installation matrix guaranteeing the correctness of camera boresight relative to inertial space. On the basis of geometric calibration, the high-accuracy image positioning can be realized and form a solid foundation for space targets tracking. Our method has been verified and applied on several satellites, such as JL-1 SP07, JL-1 SP03, and Shiyan 6-03. However, limited by the attitude accuracy of star sensor, the results of external calibration are effective but not stunning, as shown in Fig. 6(b). Therefore, the next step in this research is to fuse attitude data from more devices, such as gyros, to obtain more accurate platform attitude.

Acknowledgment

The authors would like to thank the anonymous reviews for their constructive comments and suggestions.

References

[1] L. Wang, M. Jia, D. Yin, and J. Tian, "A review of remote sensing for mangrove forests: 1956–2018," *Remote Sens. Environ.*, vol. 231, Sep. 2019, Art. no. 111223, doi: 10.1016/j.rse.2019.111223.

[2] J. J. Dalcanton, "18 years of science with the Hubble Space Telescope," *Nature*, vol. 457, no. 7225, pp. 41–50, Jan. 2009, doi: 10.1038/nature07621.
[3] J. Li, F. Xing, D. P. Chu, and Z. L. Liu, "High-accuracy self-calibration for smart, optical orbiting payloads integrated with attitude and position determination," *Sensors*, vol. 16, no. 8, pp. 1176–1195, Jul. 2016, doi: 10.3390/s16081176.
[4] Y. L. Wang, M. Wang, and Y. Zhu, "On-orbit calibration of installation parameter of multiple star sensors system for optical remote sensing satellite with ground control points," *Remote. Sens.*, vol. 12, no. 7, pp. 1055–1075, Mar. 2020, doi: 10.3390/rs12071055.
[5] T. Tadono, M. Shimada, H. Murakami, and J. Takaku, "Calibration of PRISM and AVNIR-2 onboard ALOS 'Daichi,"' *IEEE Trans. Geosci. Remote Sens.*, vol. 47, no. 12, pp. 4042–4050, Dec. 2009, doi: 10.1109/TGRS.2009.2025270.
[6] D. Mulawa, "On-orbit geometric calibration of the OrbView-3 high resolution imaging satellite," *Int. Arch. Photogramm. Remote Sens. Spatial Inf. Sci.*, vol. 35, pp. 1–6, Jul. 2004.
[7] J. Grodecki and G. Dial, "IKONOS geometric accuracy validation," *Int. Arch. Photogram. Remote Sens. Spatial Inf. Sci.*, vol. 34, no. 1, pp. 50–55, 2002.
[8] J. Grodecki and J. Lutes, "IKONOS Geometric calibrations," in *Proc. ASPRS Annu. Conf.*, 2005, pp. 1–6.
[9] R. Gachet, "SPOT5 in-flight commissioning: Inner orientation of HRG and HRS instruments," in *Proc. 20th ISPRS Congr., Commun.*, Istanbul, Turkey, vol. 35, 2004, pp. 1–5.
[10] E. Breton, A. Bouillon, R. Gacht, and F. Delussy, "Pre-flight and in-flight geometric calibration of SPOT5 HRG and HRS images," *Int. Arch. Photogramm. Remote Sens. Spatial Inf. Sci.*, vol. 34, no. 1, pp. 20–25, 2002.
[11] Y.-H. Jiang, G. Zhang, X.-M. Tang, D. Li, W.-C. Huang, and H.-B. Pan, "Geometric calibration and accuracy assessment of ZiYuan-3 multispectral images," *IEEE Trans. Geosci. Remote Sens.*, vol. 52, no. 7, pp. 4161–4172, Jul. 2014.
[12] D. Greslou, F. de Lussy, J. M. Delvit, C. Dechoz, and V. Amberg, "Pleiades-HR innovative techniques for geometric image quality commissioning," *Int. Arch. Photogramm., Remote Sens. Spatial Inf. Sci.*, vol. 1, pp. 543–547, Jul. 2012.
[13] J. M. Delevit *et al.*, "Attitude assessment using pleiades-HR capabilities," *Int. Arch. Photogramm., Remote Sens. Spatial Inf. Sci.*, vol. 1, pp. 525–530, Jul. 2012.
[14] Y. D. Pi, B. Yang, X. Li, and M. Wang, "Study of full-link on-orbit geometric calibration using multi-attitude imaging with linear agile optical satellite," *Opt. Exp.*, vol. 27, no. 2, pp. 980–998, Jan. 2019, doi: 10.1364/OE.27.000980.
[15] G. Zhang, J. Wang, Y. Jiang, P. Zhou, Y. Zhao, and Y. Xu, "On-orbit geometric calibration and validation of Luojia 1-01 night-light satellite," *Remote Sens.*, vol. 11, no. 3, p. 264, Jan. 2019, doi: 10.3390/rs11030264.
[16] G. Chander, T. J. Hewison, N. Fox, X. Wu, X. Xiong, and W. J. Blackwell, "Overview of intercalibration of satellite instruments," *IEEE Trans. Geosci. Remote Sens.*, vol. 51, no. 3, pp. 1056–1080, Mar. 2013, doi: 10.1109/TGRS.2012.2228654.
[17] J. A. Christian, L. Benhacine, J. Hikes, and C. D'Souza, "Geometric calibration of the orion optical navigation camera using star field images," *J. Astron. Sci.*, vol. 63, no. 4, pp. 335–353, Jul. 2016, doi: 10.1007/s40295-016-0091-3.
[18] S. E. Schröder *et al.*, "In-flight calibration of the dawn framing camera," *Icarus*, vol. 226, no. 2, pp. 1304–1317, Nov. 2013, doi: 10.1016/j.icarus.2013.07.036.
[19] M. Wang, Y. Cheng, B. Yang, S. Jin, and H. Su, "On-orbit calibration approach for optical navigation camera in deep space exploration," *Opt. Exp.*, vol. 24, no. 5, pp. 5536–5554, Mar. 2016, doi: 10.1364/OE.24.005536.
[20] D. Hobbes *et al.*, "Gaia DR2 documentation Chapter 2: Astrometric and photometric pre-processing," in *Proc. ESA*, Jul. 2018, p. 2.
[21] Z. Guan, Y. Jiang, J. Wang, and G. Zhang, "Star-based calibration of the installation between the camera and star sensor of the Luojia 1-01 satellite," *Remote Sens.*, vol. 11, no. 18, p. 2081, Sep. 2019, doi: 10.3390/rs11182081.
[22] M.-S. Wei, F. Xing, and Z. You, "A real-time detection and positioning method for small and weak targets using a 1D morphology-based approach in 2D images," *Light, Sci. Appl.*, vol. 7, p. 18006, May 2018, doi: 10.1038/lsa.2018.6.
[23] Z. Z. Chen *et al.*, "Multimorphological top-hat-based multiscale target classification algorithm for real-time image processing," *Appl. Opt.*, vol. 58, no. 22, pp. 6045–6056, 2019, doi: 10.1364/AO.58.006045.
[24] R. L. Newburn, "Stardust imaging camera," *J. Geophys. Res.*, vol. 108, no. E10, p. 8116, 2003, doi: 10.1029/2003JE002081.
[25] Z. Guan, G. Zhang, and L. Ge, "Correction of camera interior orientation elements based on multi-frame star map," in *Proc. IEEE Int. Geosci. Remote Sens. Symp.*, Oct. 2020, pp. 6238–6241, doi: 10.1109/IGARSS39084.2020.9323389.
[26] S. A. Klioner, "A practical relativistic model for microarcsecond astrometry in space," *Astronomical J.*, vol. 125, no. 3, pp. 1580–1597, Mar. 2003, doi: 10.1086/367593.
[27] J. A. Christian, "StarNAV: Autonomous optical navigation of a spacecraft by the relativistic perturbation of starlight," *Sensors*, vol. 19, no. 19, pp. 4064–4126, Sep. 2019, doi: 10.3390/s19194064.
[28] *The Hipparcos and Tycho Catalog: Introduction and Guide to the Data*, document SP-1200, ESA, 1997.
[29] L. Lindegren, U. Lammers, D. Hobbs, W. O'Mullane, U. Bastian, and J. Hernández, "The astrometric core solution for the Gaia mission: Overview of models, algorithms, and software implementation," *Astron. Astrophys.*, vol. 538, p. A78, Feb. 2012, doi: 10.1051/0004-6361/201117905.
[30] M. D. Shuster, "Stellar aberration and parallax: A tutorial," *J. Astron. Sci.*, vol. 51, no. 4, pp. 477–494, Dec. 2003, doi: 10.1007/BF03546295.
[31] J. Meeus, *Astronomical Algorithms*, 2nd ed. Richmond, VA, USA: Willmann-Bell, 1999.
[32] X. Shen, B. Liu, and Q.-Q. Li, "Correcting bias in the rational polynomial coefficients of satellite imagery using thin-plate smoothing splines," *ISPRS J. Photogramm. Remote Sens.*, vol. 125, pp. 125–131, Mar. 2017, doi: 10.1016/j.isprsjprs.2017.01.007.
[33] E. Hog *et al.*, "The Tycho-2 catalogue of the 2.5 million brightest stars," *Astron. Astrophys.*, vol. 355, pp. 27–30, Jan. 2000.

Xuedi Chen (Graduate Student Member, IEEE) was born in 1997. He received the B.S. degree in measurement and control technology and instrument from the School of Precision Instrument and Optoelectronics Engineering, Tianjin University, Tianjin, China, in 2018. He is currently pursuing the Ph.D. degree with the Department of Precision Instrument, Tsinghua University.

His research interest includes geometry processing of spaceborne optical imagery.

Fei Xing received the B.S. degree in mechanical engineering degree from Tongji University, Shanghai, China, in 2002, and the Ph.D. degree from Tsinghua University, Beijing, China, in 2006.

After graduation, he joined the Faculty of the Department of Precision Instruments and Mechanology, Tsinghua University, as an Assistant Researcher, where he became an Associate Professor in 2011. He has published more than 70 articles. His main research interests include microminiature high-precision attitude measurement sensor technology.

Dr. Xing awarded the specially appointed Professor for Chang Jiang Scholar from the Ministry of Education in 2020.

Zheng You received the B.S., M.S., and Ph.D. degrees from the Huazhong University of Science and Technology, Wuhan, China, in 1985, 1987, and 1990, respectively.

After graduation, he joined the Faculty of the Department of Precision Instruments and Mechanology, Tsinghua University, Beijing, China, as an Assistant Professor, where he became an Associate Professor in 1992 and a Full Professor in 1994. In 2015, he was the Vice President of Tsinghua University. He has published more than 300 articles and 32 research reports. He holds 12 Chinese invention patents. His main research interests include microtechnology–nanotechnology and micro–nano satellite technology.

Dr. You awarded the specially appointed Professor for Chang Jiang Scholar from the Ministry of Education in 2001 and the Academician by the Chinese Academy of Engineering in 2013.

Xing Zhong received the Ph.D. degree in optical engineering from the Changchun Institute of Optics, Fine Mechanics and Physics (CIOMP), Changchun, China, in 2009.

He worked at CIOMP as an Associate Professor from 2009 to 2014. In 2015, he became a Full Professor at CIOMP and took part in the work for founding Chang Guang Satellite Technology Company Ltd. (CGSTL), Changchun. He is currently the Vice President and the Chief Engineer with CGSTL and a Professor at the University of Chinese Academy of Sciences, Beijing, China. His research interest is satellite's overall design, especially the payload and platform integration technologies.

Kaihua Qi received the B.S. degree in aircraft design engineering and the M.S degree in aerospace engineering from Northwestern Polytechnical University, Xi'an, China, in 2012 and 2015, respectively.

He is currently engaged in high-precision and high-stability satellite attitude control technology.